

Differential capacitance and electrochemical impedance study of surfactant adsorption on polycrystalline Ni electrode

A. G. Anastopoulos¹ · A. D. Papoutsis¹ · A. A. Papaderakis¹

Received: 17 November 2014 / Revised: 28 April 2015 / Accepted: 6 May 2015 / Published online: 17 May 2015
© Springer-Verlag Berlin Heidelberg 2015

Abstract The adsorption of neutral organophosphorous compounds on a charged polycrystalline Ni electrode is studied by differential capacitance and impedance measurements in methanol solutions. Analysis of capacitance measurements reveals that tributylphosphine oxide, tri(*n*)octylphosphine oxide, and triphenylphosphine follow Langmuir adsorption isotherm. Saturation capacitance C_{sat} , potential of maximum adsorption E_{max} , limiting surface concentration Γ_{max} , and standard Gibbs energy of adsorption $\Delta G_{\text{max}}^{\circ}$ at E_{max} are determined. The cathodic reduction of $(\text{NiOCH}_3)_{\text{ads}}$ film formed on Ni surface at positive potentials, introducing a faradaic contribution in addition to the electrostatic charging of the interface, is supported by linear sweep voltammetric and impedance measurements. High values of electrode coverage and strong depression of faradaic currents are attained, indicating that these adsorbates may be suitable as corrosion inhibitors.

Keywords Nickel electrode · Organophosphorus · Inhibitors · Capacitive charging · Irreversible adsorption · Non-capacitive response

Introduction

Nickel in the form of pure bulk metal or as an alloy constituent or finely divided as nanoparticles and nanopowder or in the form of nickel hydride and nickel oxide is used as an electrode

material in important electrochemical applications including batteries, fuel cells and electrochemical capacitors, catalysis of electrode reactions, electroplating, protection against corrosion, transformation of solar energy, etc.

The operation of metal electrodes is principally the result of the specific characteristics of the electrode/solution interface, which can be probed by the adsorption of surface active ionic and non-ionic species. In the case of nickel electrodes, such adsorption studies, appearing in the literature for almost the last 40 years, were usually based on radiotracer techniques [1], on the electrochemical quartz microbalance technique [2] and also on spectroscopic methods [3–5].

A survey of the voltammetric, kinetic, and double layer studies of nickel electrodes up to 1971 presented by Arvia and Posadas [6] and a more recent review by Inzelt and Horanyi [7] revealed that adsorption studies by means of electrochemical impedance and differential capacitance are very rare with the exception of a few papers of Bockris and Devanathan [8, 9] reporting complete C – E curves and other publications [10] reporting indicative capacitance values.

In our present work, we investigate the interface of a polycrystalline Ni electrode in contact with neutral methanolic solutions containing non-ionic organophosphorus adsorbates by means of differential capacitance and electrochemical impedance measurements. Methanol is an efficient solvent for all organophosphorus compounds. Organophosphorus and related compounds constitute a family of surfactants which can be effectively used as probes to obtain information about metal/solution interface.

The advantages of organophosphorus compounds refer to their solubility in a variety of solvents, their significant adsorbability and the width of adsorption potential region, and their electrochemical stability and strong inhibitory action on various electrode reactions as for example the electroreduction of metal cations at the Hg electrode in a

✉ A. G. Anastopoulos
anasto@chem.auth.gr

¹ Department of Chemistry, Aristotle University of Thessaloniki, 54124 Thessaloniki, Greece

variety of solvents. Due to their inhibitory action, organophosphorus compounds may be proved to act as effective corrosion inhibitors. Among them, triphenylphosphine oxide and triphenylarsine oxide were frequently used as reaction inhibitors [11] and also as probes of Hg/solution [12, 13] and Ag/solution interface [14], while other alkyl substituted phosphinoxides [11], phosphines, arsines [15], and phosphonium salts [16, 17] have received less attention.

Experimental

Polycrystalline Ni working electrode was assembled by using a nickel rod (Goodfellow, purity 99 %) embedded in a glass cylinder, sealed by adhesive resistant to water and methanol, and covered with thermoplastic tube, so as to leave at its end an insulated disk surface of 3-mm diameter.

A Pt foil was used as auxiliary electrode, the free end of which was bended so as to be parallel to the disk face of the working electrode at a distance of about 2 mm, in order to ensure uniform potential distribution.

In all measurements, an aqueous Schott reference Ag|AgCl electrode saturated with NaCl was used and placed at a distance of less than 5 mm from both working and auxiliary electrodes without the use of Luggin capillary. The electrode arrangement was set in a single compartment double-walled electrochemical cell kept at 298 K. LiClO₄ (0.1 M) in methanol is used as base solution in all measurements.

The working electrode was mechanically polished by Al₂O₃, then it was rinsed with distilled water and chemically cleaned and polished in aqueous 10 % v/v HNO₃. After that, it was set for several minutes in an ultrasonic bath containing distilled water, and then, it was washed with the working solution and transferred to the electrochemical cell, taking care to avoid contact with air. Then, by means of linear sweep voltammetry (LSV), the working electrode was scanned from 0.3 to -0.8 V vs. Ag|AgCl with a rate of 0.25 V s⁻¹.

LSV scans and electrochemical impedance spectroscopy (EIS) measurements were carried out by the electrochemical system Autolab PGSTAT302N connected to a personal computer running the Autolab software necessary for the control of LSV and EIS measurements. EIS measurements were carried out within a frequency range of 1 Hz to 10 kHz with 4-mV ac signal at various dc potentials.

Capacitance measurements were carried out by the experimental setup described previously [18], which comprises a lock-in amplifier (model SR830 from Stanford Research) and a potentiostat (model Potentiostat Wenking POS73 from Bank Elektronik), interfaced to our personal computer running LabVIEW 6.1 under Windows XP. The dc potential was applied in steps of 25 mV, and each measurement was taken after a 5-s stopover at each potential. The amplitude and

the frequency of the ac signal were set to 4 mV and 80 Hz, respectively.

The standard deviation between at least three successive capacitance measurements, expressed on a percent basis, was found to be on average equal to about 5 % within the potential range from 0.3 to -0.70 V vs. Ag|AgCl. In this respect, the reproducibility of our measurements may be considered as a reasonable one.

The reproducibility of all electrochemical impedance measurements confirmed by the comparison of two to three successive measurements at the same potential was very satisfactory over all the frequency range.

The linearity-stability of EIS measurements was checked by the Kramers-Kronig test incorporated in the Autolab software by which the complex, the real, and the imaginary pseudo-chi-squared were found to be of the order of 10⁻⁵ to 10⁻⁶ in all systems studied and over all the frequency range used.

The chemical reagents used without further purification are anhydrous LiClO₄ (Aldrich 99.99 %), tributylphosphine oxide (TBPO, Aldrich), tri(*n*)octylphosphine oxide (TOPO, Merck), triphenylphosphine (TPP, Fluka), and methanol (MeOH, Lab-Scan, purity >99 %, maximum water content 0.05 %).

Results and discussion

Differential capacitance curves of the interface between polycrystalline Ni and methanol solutions of TBPO, TOPO, and TPP are shown in Figs. 1, 2, and 3. Capacitance values are expressed with respect to the geometrical area of the working electrode.

The overall profile of the base electrolyte capacitance vs. potential curve of the working Ni electrode in methanolic solution of 0.1 M LiClO₄ approximates that of Bockris [8]

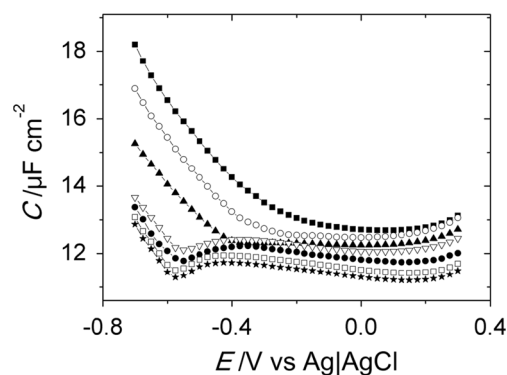


Fig. 1 Differential capacitance curves of polycrystalline Ni in contact with methanolic solutions of 0.1 M LiClO₄ containing the following tributylphosphine oxide concentrations in molar: 0 (black square), 0.0025 (white circle), 0.005 (black up-pointing triangle), 0.01 (white down-pointing triangle), 0.02 (black circle), 0.04 (white square), and 0.06 (black star)

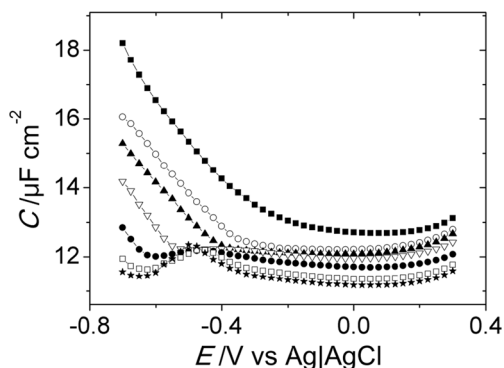


Fig. 2 Differential capacitance curves of polycrystalline Ni in contact to methanolic solutions of 0.1 M LiClO₄ containing the following tri(n)octylphosphine oxide concentrations in molar: 0 (black square), 0.0025 (white circle), 0.005 (black up-pointing triangle), 0.01 (white down-pointing triangle), 0.02 (black circle), 0.04 (white square), and 0.05 (black star)

and Devanathan [9] in aqueous solutions. Moreover, the minimum capacitance of 12.7 μF cm⁻² in methanol and 19.3 μF cm⁻² in aqueous 0.1 M LiClO₄, the latter obtained by preliminary experiments, is in reasonable agreement with the corresponding values of 18.5–19.5 μF cm⁻² provided by Bockris in aqueous solutions of KClO₄–NaOH mixtures. Within the potential range from 0.3 to –0.7 V vs. Ag|AgCl, the base electrolyte capacitance curve of Ni in 0.1 M LiClO₄ in methanol presents no particular features.

The minimum is located at E=0.075 V vs. Ag|AgCl close to the minimum of the aqueous solution at 0.05 V vs. Ag|AgCl and to the value of –0.26 V vs. normal hydrogen electrode (NHE) of the potential of zero charge in aqueous perchlorate solutions reported by Bockris [8] and also to the average value of –0.3 V vs. NHE reported by Trasatti [19]. The small increase of capacitance at potentials close to 0.3 V vs. Ag|AgCl may be caused by weak adsorption of perchlorate ions. On the other hand, the increase of capacitance values negative to –0.2 V vs. Ag|AgCl may be of faradaic origin. On account of the LSV curves of the base solution, shown in Fig. 4,

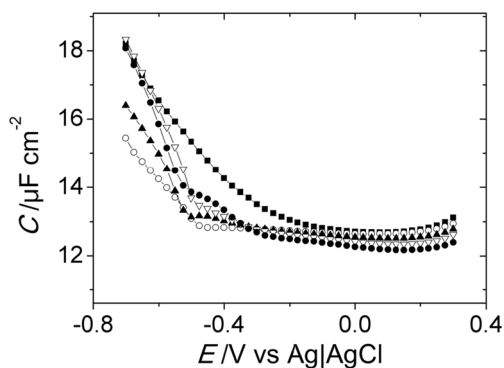


Fig. 3 Differential capacitance curves of polycrystalline Ni in contact to methanolic solutions of 0.1 M LiClO₄ containing the following triphenylphosphine concentrations in molar: 0 (black square), 0.005 (white circle), 0.01 (black up-pointing triangle), 0.02 (white down-pointing triangle), and 0.04 (black circle)

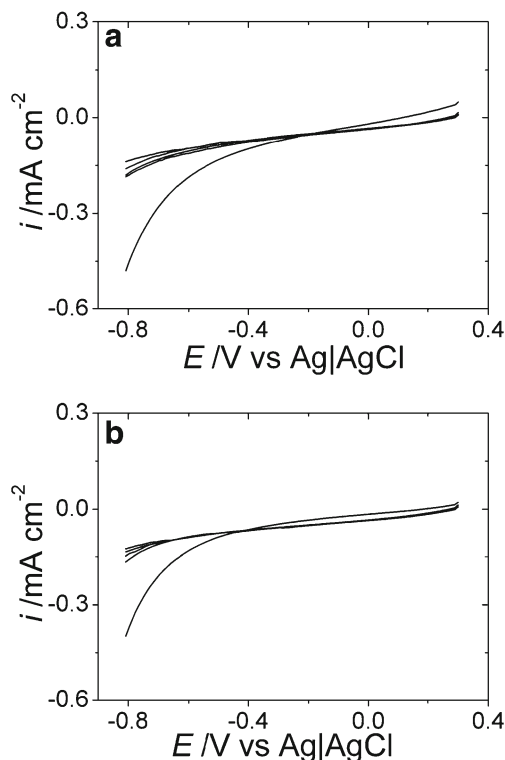
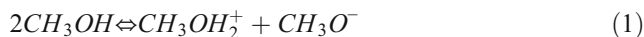


Fig. 4 Linear sweep voltammetric curves of polycrystalline Ni in contact to methanolic solutions of 0.1 M LiClO₄ containing **a** tributylphosphine oxide and **b** tri(n)octylphosphine oxide concentrations in molar (bottom to top): 0, 0.005, 0.01, 0.02, and 0.04. Potential scan rate=0.25 V s⁻¹

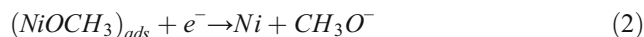
the increase of cathodic current suggests for the occurrence of a charge transfer reaction negative to –0.2 V vs. Ag|AgCl.

To identify this reaction, we must account for the conditions prevailing on Ni surface in methanolic LiClO₄ solutions. From a variety of descriptions regarding anodic film formation on Ni surface over all the pH range [20, 21], we suggest that in anhydrous neutral solutions, methanol is auto-dissociated [22] according to the scheme:



resulting to the coverage of Ni surface by methoxy anions.

At anodic polarizations, (NiOCH₃)_{ads} is formed on the electrode surface, which at negative potentials is reduced as:



giving rise to the observed increase of cathodic current. In this respect, the charging process of the Ni/methanolic solution interface is not of purely electrostatic character, but it is also contributed by a faradaic process such as reaction (2). As long as in neutral solutions hydrogen evolution reaction (HER) sets on at potentials neighboring and negative to –0.9 V vs. Ag|AgCl, it is presumed that reaction (2) precedes HER.

Returning to the capacitance curves, TBPO, TOPO, and TPP seem to have a more or less similar effect on the

capacitance of Ni/methanol interface. In the presence of TBPO and TOPO capacitance, curves are regularly depressed within the potential range from 0.3 to -0.3 V vs. Ag|AgCl followed, when adsorbate concentration exceeds 0.005 M, by a fluctuation observed at negative potentials close to -0.4 V vs. Ag|AgCl. This fluctuation has the form of a hump, and it is stronger in the case of TOPO tending to form a broad peak, the height of which is increasing with adsorbate concentration.

Negative to the hump, a strong increase of capacitance values is observed, and capacitance curves shift to more negative potentials by increasing adsorbate concentration. Coincidence of capacitance curves in the presence of adsorbate with that of the base electrolyte is far from being observed.

According to the theory of Frumkin [23, 24], capacitance fluctuations in the form of humps and peaks are interpreted in terms of interfacial structural changes leading to the recession of dielectric saturation in the adsorbed layer, resulting either from adsorption–desorption processes of adsorbed particles or from superficial rearrangements including reorientation.

It may be assumed that at negative potentials, such as -0.4 V vs. Ag|AgCl, the reorientation of adsorbed phosphine oxides does not seem to be a reasonable possibility, and desorption of TBPO and TOPO is more possible. Therefore, the increase of capacitance values at these potentials, in adsorbate-containing solutions, may be justified similarly to the base solution.

In the presence of TPP, the regularity of capacitance curves of Figs. 1 and 2 negative to -0.4 V vs. Ag|AgCl is distorted. Humps are replaced with a shoulder-like variation of capacitance, and above 0.01 M capacitance, curves merge with that of base solution at potentials negative to -0.5 V vs. Ag|AgCl, which apparently seems to be the result of TPP desorption. However, the occurrence of a faradaic reaction involving TPP at potentials negative to -0.4 V vs. Ag|AgCl may be an alternative interpretation.

LSV curves of Fig. 4 show the strong depression of faradaic current over all the potential range of TBPO and TOPO adsorption. This is an indication in support of the inhibitory influence of adsorbed phosphinioxides on electrode reactions occurring at negative potentials.

At potentials negative to -0.4 V vs. Ag|AgCl, it is seen that the faradaic current in TBPO- and TOPO-containing solutions is increasing. This means that reaction (1) is no longer retarded due to the assumed desorption of TBPO and TOPO.

In the presence of TPP (Fig. 5), depression of the faradaic current is apparently limited at concentrations below 0.02 M. With the increase of TPP content above 0.005 M, cathodic current is seen to re-increase and the potential profile of LSV curves is markedly changing. This is possibly the result of a charge transfer reaction

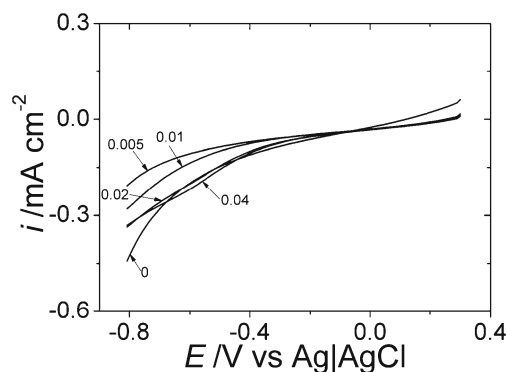


Fig. 5 Linear sweep voltammetric curves of polycrystalline Ni in contact to methanolic solutions of 0.1 M LiClO₄ containing the following triphenylphosphine concentrations in molar: 0, 0.005, 0.01, 0.02, and 0.04, as noted on the plot. Potential scan rate = 0.25 V s⁻¹

involving TPP, which may be assumed to be reduced at a first step according to the scheme [25]:



In any case, the discussion about the interfacial processes which manifest themselves on the C - E and LSV curves makes necessary the determination of interfacial parameters which can be accessed either directly from the experimental adsorption isotherms or subsequently by the application of isotherm analysis.

Isotherm analysis is based on capacitance measurements in terms of the known equation resulting from the theory of Frumkin and Damaskin [26]:

$$C_i = C_o(1-\theta) + C_{\text{sat}}\theta + (q_{\text{sat}} - q_o) \frac{d}{dE} \quad (4)$$

In Eq. (4), θ is the degree of electrode coverage, C_o and q_o are the capacitance and surface charge density in the absence of adsorbate, C_i is the capacitance in the presence of an intermediate adsorbate concentration, and C_{sat} and q_{sat} are the capacitance and surface charge density corresponding to the condition $\theta=1$. C_{sat} is calculated by extrapolation of $1/C_i$ vs. $1/c_A$ plots at infinite bulk adsorbate concentration c_A .

Strictly speaking, the degree of electrode coverage can be calculated by Eq. (4) within the potential range where the condition $d\theta/dE=0$ is satisfied. However in practice, the calculation of electrode coverage is carried out within the potential range where the condition $dC_i/dE \approx 0$ is satisfied. In Figs. 1, 2, and 3, this is approximately true at either sides of the anodic minimum of the C - E curves, viz. within the potential range from 0.3 to -0.3 V vs. Ag|AgCl for TBPO and TOPO and 0.3 to -0.2 V vs. Ag|AgCl for TPP. Thus, the degree of electrode coverage is of apparent nature, and henceforth it is denoted by θ_{app} .

Isotherm analysis confirms that all systems studied are in very satisfactory agreement with the theoretical Langmuir isotherm:

$$BC_A = \frac{\theta_{app}}{1-\theta_{app}} \tag{5}$$

at electrode potentials ranging from 0.3 to -0.1 V vs. Ag|AgCl. At potentials more negative than -0.1 V vs. Ag|AgCl, the linearity of the isotherm test $1/\theta_{app}$ vs. $1/c_A$ plots markedly deteriorates ($R^2 < 0.95$), and the Langmuir isotherm is no longer valid. This is also true for the Frumkin isotherm over all the potential range studied.

In Eq. (5), B is the adsorption equilibrium constant, related to the electrode potential E by means of equation [26]:

$$B = \frac{1}{c_s} \exp\left(-\frac{\frac{1}{2}(C_0 - C_{sat})E^2 + C_{sat}E_N E}{RT\Gamma_{max}}\right) \tag{6}$$

In Eq. (6), c_s is the bulk solvent concentration, E_N is the displacement of the zero charge potential due to the adsorption of ionic and polar non-ionic species, and Γ_{max} is the limiting surface adsorbate concentration corresponding to the potential of maximum adsorption, E_{max} .

At a first approximation, E_{max} is the potential corresponding to the maximum value of the apparent electrode coverage. The potential dependence of θ_{app} obtained for the studied adsorbates by the application of Eq. (4) at various potentials and preferentially at higher bulk adsorbate concentrations is shown in Fig. 6.

It must be pointed that condition $d\theta/dE=0$ is satisfactorily valid only at the direct vicinity (viz. ± 50 mV) of the potential of maximum adsorption, E_{max} , where the adsorption parameters of Table 1 are calculated. At a more extended potential range, the potential profile of electrode coverage shown in Fig. 6 is of apparent and indicative character. In Fig. 6, we may point out that, in the presence of TPP, electrode coverage

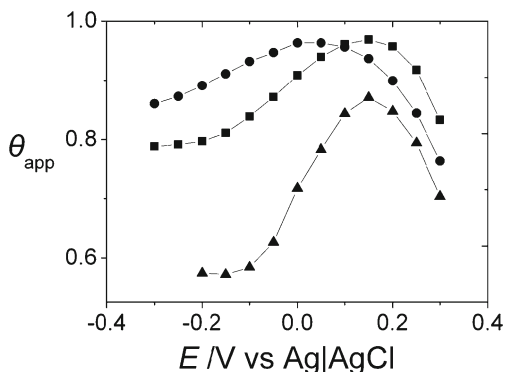


Fig. 6 Potential dependence of apparent electrode coverage in the presence of 0.06 M TBPO (black square), 0.05 M TOPO (black circle), and 0.04 M TPP (black up-pointing triangle)

Table 1 Interfacial parameters of TBPO, TOPO, and TPP

Adsorbate	C_{sat} $\mu\text{F cm}^{-2}$	E_{max} V vs. Ag AgCl	Γ_{max} mol cm^{-2}	ΔG_{max}° kJ mol^{-1}
TBPO	11.2	0.15	8.8×10^{-11}	18.3
TOPO	11.1	0.05	5.0×10^{-11}	20.6
TPP	12.1	0.15	6.3×10^{-11}	17.5

markedly decreases at negative potentials. However, it is observed that θ_{app} of TPP is reduced but not zeroed, which means that adsorbed TPP is not completely desorbed but possibly undergoes a structural reorganization. At such negative potentials, phosphorous atom may be brought closer or even in contact to the electrode surface. Equation (6) can be simplified by setting $E_N \approx 0$, which is a reasonable approximation for polycrystalline electrodes [24, 27]. Then, by taking logarithms of both sides, we obtain:

$$\ln B = \ln\left(\frac{1}{c_s}\right) - \frac{(C_0 - C_{sat})}{2RT\Gamma_{max}E^2} \tag{7}$$

The limiting surface concentration Γ_{max} is calculated in terms of Eq. (7), by applying linear regression to the $\ln B$ vs. E^2 plots, shown in Fig. 7.

This method is applicable only within a monotonic range of potentials. In the case of TBPO, TOPO, and TPP, this is the range of potentials from 0.0 to 0.3 V vs. Ag|AgCl.

The calculated values of Γ_{max} together with the corresponding values of C_{sat} , E_{max} , and ΔG_{max}° are provided in Table 1. The tabulated values of Γ_{max} and ΔG_{max}° correspond to the potential of maximum adsorption, E_{max} .

The agreement of TBPO, TOPO, and TPP adsorption data with the theoretical Langmuir isotherm is indicatively demonstrated at E_{max} by the $1/\theta_{app}$ vs. $1/c_A$ plots of Fig. 8.

The identification of processes occurring at the Ni/solution interface is further assisted by EIS measurements. Within the potential range from 0.3 to -0.2 V vs. Ag|AgCl, spectra

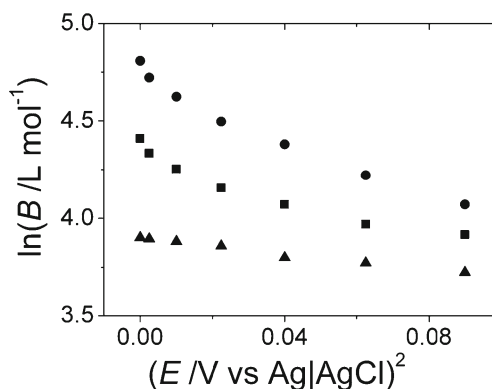


Fig. 7 Dependence of the logarithm of adsorption equilibrium constant on the square of electrode potential in the presence of 0.06 M TBPO (black square), 0.05 M TOPO (black circle), and 0.04 M TPP (black up-pointing triangle)

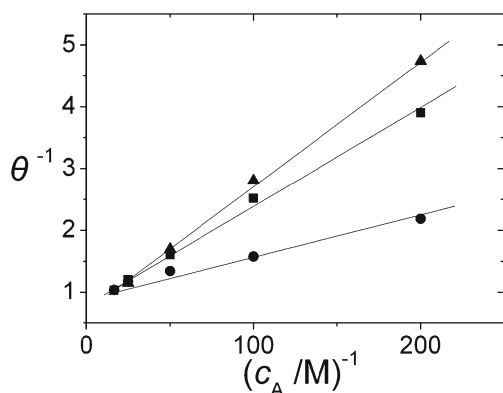


Fig. 8 Test of the Langmuir adsorption isotherm at the potential of maximum adsorption of TBPO (black square), TOPO (black circle), and TPP (black up-pointing triangle)

shown in Fig. 9 markedly deviate from the vertical line representing an ideal capacitor with no parallel resistance. Moreover, these plots are slightly curved but do not present an unambiguous form of semicircle.

In the absence of TBPO, TOPO, and TPP, the complex plane impedance plots of Figs. 9 and 10 show an increase of curvature at potentials negative to -0.2 V vs. Ag|AgCl. Particularly, at potentials more negative than -0.4 V vs. Ag|AgCl, plots of $-Z''$ vs. Z' tend to the formation of semicircles. This finding suggests for a joint effect of the double layer capacitance and the increasing contribution of a charge transfer resistance with increasing negative potentials as the result of process (2) in agreement to the LSV plots of Figs. 4 and 5.

Within the potential range from 0.3 to -0.2 V vs. Ag|AgCl, the deviation of the $-Z''$ vs. Z' plots from the vertical line is increasing with the introduction of TBPO and TOPO but not in the presence of TPP except of the $-Z''$ vs. Z' plot of Fig. 9c at $E = -0.2$ V vs. Ag|AgCl.

At even more negative potentials, the form of impedance spectra is changed. As shown in Fig. 11 in the presence of TOPO and TBPO, the deviation from the vertical line is no longer greater than that of the base solution. Possibly due to the change of the structure of the adsorption layer associated with the observed capacitance hump at -0.4 to -0.5 V vs. Ag|AgCl, impedance spectra in the presence of TBPO and TOPO tend to overtop that of the base electrolyte. In the presence of TPP, a single incomplete semicircle is obtained, denoting the occurrence of a charge transfer process, which is already identified with reaction (3).

This is an indication that a single reaction is clearly detected only in the presence of TPP and not in the presence of TBPO and TOPO, possibly because the presumed shift of phosphorus atom closer to the negatively charged Ni surface favors the electron uptake by the TPP molecule.

In the preceding discussion, it was assumed that the overall charging process of the interface includes an

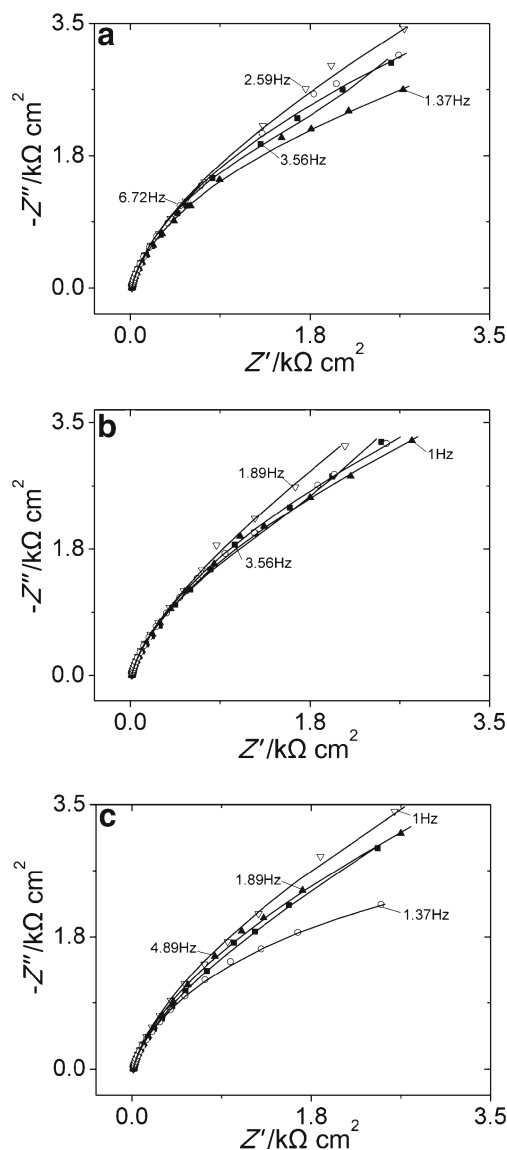


Fig. 9 Experimental complex plane impedance plots of polycrystalline Ni in contact to methanolic solutions of 0.1 M LiClO₄ in the absence (white down-pointing triangle) and in the presence of 0.04 M TBPO (black square), TOPO (black up-pointing triangle), and TPP (white circle) at the following electrode potentials: **a** 0.3, **b** 0.0, **c** -0.2 V vs. Ag|AgCl. Solid lines represent impedance spectra calculated from the model of Fig. 12a in the case of base solution, TBPO, TOPO, and for TPP only at potentials 0.3 and 0.0 V vs. Ag|AgCl. At -0.2 V vs. Ag|AgCl in the presence of TPP calculated spectra refer to the model of Fig. 12b

electrostatic as well as a faradaic contribution, the latter associated with reaction (2).

In connection to this assumption, impedance data, within the potential range 0.3 to -0.2 V vs. Ag|AgCl, are treated by means of the equivalent circuit shown in Fig. 12a, which results from the modification of the standard adsorption model [28]. This circuit comprises the solution resistance, R_S , in series with the parallel combination of two CPEs. One of them, denoted CPE-1, stands for the contribution of the double layer capacitance. The second one, denoted CPE-2, stands

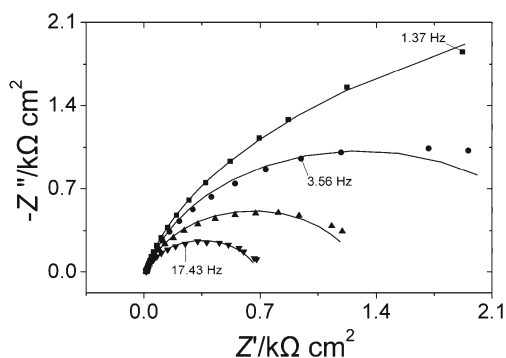


Fig. 10 Experimental complex plane impedance plots of polycrystalline Ni in contact to the base solution at the following electrode potentials: -0.4 (black square), -0.5 (black circle), -0.6 (black up-pointing triangle), and -0.7 (black down-pointing triangle) V vs. Ag|AgCl. Solid lines represent impedance spectra calculated from the model of Fig. 12a

for the non-capacitive response of the interface due to faradaic processes involving adsorbed species. In this respect, CPE-2 is connected in series with the charge transfer resistance, R_{ct} , corresponding to reaction (2).

The impedances Z_{CPE-1} of CPE-1 and Z_{CPE-2} of CPE-2 are expressed by the relations:

$$Z_{CPE-1} = \frac{1}{Y_{o1}(j\omega)^{n_1}} \text{ and } Z_{CPE-2} = \frac{1}{Y_{o2}(j\omega)^{n_2}} \quad (8)$$

where Y_{o1} , Y_{o2} , and n_1 , n_2 are, respectively, the corresponding pre-exponential factors and CPE exponents.

In this respect, experimental impedance data were fitted to the circuit of Fig. 12a by means of a complex nonlinear least squares (CNLS) routine incorporated in the NOVA 1.11 control software of the Autolab system. The mean fitting quality of the experimental spectra, expressed by the factor χ^2 , is of the order of 10^{-3} , which is reasonable for a polycrystalline electrode.

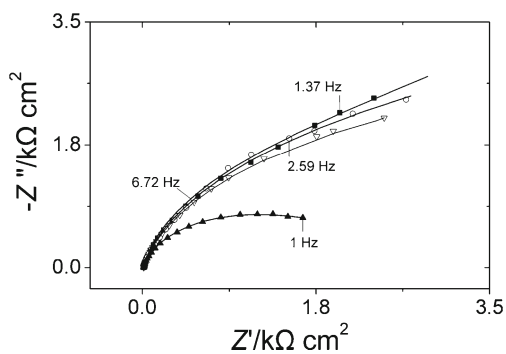


Fig. 11 Experimental complex plane impedance plots of polycrystalline Ni in contact to methanolic solutions of 0.1 M LiClO₄ in the absence (white down-pointing triangle) and in the presence of adsorbates: TBPO (black square), TOPO (white circle), and TPP (black up-pointing triangle). Adsorbate concentration 0.04 M. Electrode potential -0.4 V vs. Ag|AgCl. Solid lines represent impedance spectra calculated from the model of Fig. 12a for base electrolyte, TBPO, and TOPO and from model 12b for TPP

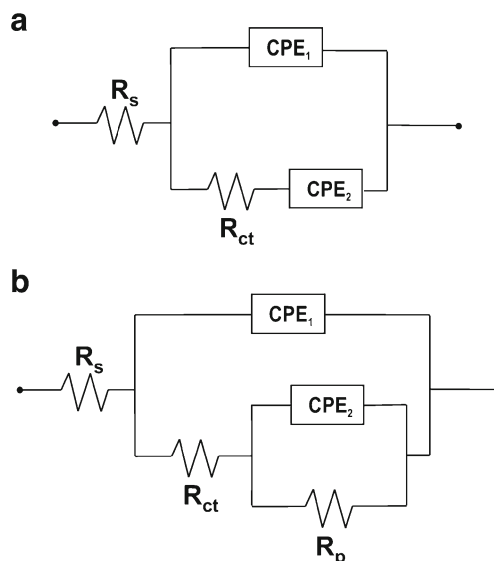


Fig. 12 Equivalent circuits based on variants of the standard adsorption model: **a** used for fitting experimental EIS data in the absence and in the presence of TBPO and TOPO within the potential range from 0.3 to -0.4 V vs. Ag|AgCl and in the presence of TPP at potentials 0.3 and 0.0 V vs. Ag|AgCl and **b** in the presence of TPP at potentials -0.2 and -0.4 V vs. Ag|AgCl

The results of the CNLS fitting are provided in Table 2. As expected, in all cases, the pre-exponential factor Y_{o1} is always much less than Y_{o2} . Table 2 also shows that CPE-1 exponent n_1 is always equal to or greater than 0.89 in agreement to its almost capacitive behavior. On the other hand, values of n_2 , ranging between 0.3 and 0.54, at a first approximation may be typically identified with a Warburg element representing semi-infinite planar diffusion.

However, on account of the absence of a capacitive element (due to a reversible adsorption process) in the faradaic branch [29] of the equivalent circuit of Fig. 12a, such n_2 values can be reasonably described in terms of a non-ideally reversible adsorption process such as the formation of $(NiOCH_3)_{ads}$.

Moreover, Table 2 shows that, in agreement to capacitance and LSV data in the absence of surfactants, R_{ct} is reduced. This means that reaction (2), as expected, is favored by the increase of negative potential.

In TBPO- and TOPO-containing solutions, LSV data suggest that no faradaic reaction due to these surfactants is detected. In this case, R_{ct} is increasing with respect to base solution, being always greater than the R_{ct} of the surfactant-uncovered electrode surface.

In the presence of TPP according to Table 2, within the potential range 0.3 to -0.2 V vs. Ag|AgCl, R_{ct} values are lower than those of TBPO and TOPO. This may be explained by assuming that the lower electrode coverage attained by TPP results to more adsorption sites available for the adsorption of methanol molecules on the electrode surface. On the other hand, the difference between the R_{ct} in the base solution with that in presence of TPP is

Table 2 CNLS results derived from equivalent circuit 12a in the absence (base solution) and in the presence of TBPO and TOPO and only for potentials 0.3 and 0.0 V vs. Ag|AgCl for TPP and from equivalent circuit 12b for TPP at potentials -0.2 and -0.4 V vs Ag|AgCl. Adsorbate concentration of 0.04 M

E V vs. Ag/AgCl	Adsorbate	R_s $\Omega \text{ cm}^2$	n_1	$Y_{o,1}$ $10^6 \Omega^{-1} \text{ s}^{n_1} \text{ cm}^{-2}$	n_2	$Y_{o,2}$ $10^6 \Omega^{-1} \text{ s}^{n_1} \text{ cm}^{-2}$	R_{ct} $\text{k}\Omega \text{ cm}^2$
0.3	b.s.	13.9	0.93	18.4	0.42	81.7	1.2
	TBPO	13.4	0.90	22.4	0.54	94.6	2.8
	TOPO	14.1	0.91	20.5	0.39	129.5	1.8
	TPP	13.5	0.93	19.4	0.33	96.9	0.5
0.0	b.s.	13.8	0.93	18.4	0.47	66.2	1.4
	TBPO	13.4	0.90	22.2	0.48	85.4	2.2
	TOPO	14.0	0.91	20.2	0.40	91.3	1.7
	TPP	13.4	0.93	19.7	0.37	86.5	0.7
-0.2	b.s.	13.8	0.92	19.5	0.40	79.1	0.9
	TBPO	13.3	0.90	22.8	0.45	94.0	1.6
	TOPO	14.0	0.91	19.7	0.38	91.0	1.0
	TPP	13.4	0.93	20.7	0.36	113.4	0.6
-0.4	b.s.	13.8	0.91	23.8	0.24	150.0	0.1
	TBPO	13.4	0.92	17.6	0.42	125.8	2.0
	TOPO	14.0	0.92	18.8	0.28	129.8	0.3
	TPP	13.4	0.93	20.5	0.40	201.0	0.6

b.s. base solution

difficult to be explained unless an interaction between reaction (2) and (3) is adopted.

At potentials more negative than -0.2 V vs. Ag|AgCl, impedance data are fitted to the equivalent circuit shown in Fig. 12b. In this case, the parallel resistance R_p has a charge transfer character and is related to the reduction of the adsorbed TPP molecules according to reaction (3), while all the other circuit elements maintain the same character as in circuit 12a.

Generally, it would be expected that by increasing negative potential, R_{ct} is gradually reduced. However, this is not confirmed by the analysis of impedance data according to circuit 12b. It is found that R_{ct} , at -0.2 V vs. Ag|AgCl, remains necessarily unchanged relatively to the corresponding TPP results at more positive potentials. This may be attributed to the parallel and possibly competitive character of reactions (2) and (3).

Table 3 Experimental differential capacitance and CPE-1 parameters of the Ni/0.1 M LiClO₄ methanolic solution interface in the absence of adsorbates

E V vs. Ag/AgCl	C $\mu\text{F cm}^{-2}$	$Y_{o,1}$ $10^6 \Omega^{-1} \text{ s}^{n_1} \text{ cm}^{-2}$	n_1
0.3	13.1	18.4	0.93
0.0	12.7	18.4	0.93
-0.2	13.1	19.5	0.92
-0.4	14.3	23.8	0.91

The onset of reaction (3) may be detected at potentials negative to 0.0 V vs. Ag|AgCl as presumed from the R_p values of 19.5 and 2.7 $\text{k}\Omega \text{ cm}^2$ obtained at -0.2 and -0.4 V vs. Ag|AgCl, respectively.

The above R_p values are much higher than the value of $R_{ct}=0.6 \text{ k}\Omega \text{ cm}^2$ corresponding to reaction (2) at the same potentials. This may be a reflection of the assumed interaction between reactions (2) and (3).

The discrimination between the electrostatic charging and the non-capacitive response of the interface, enabled by fitting impedance data to the equivalent circuit of Fig. 12a, allows for the comparison of capacitance values measured by the lock-in system with $Y_{o,1}$ values calculated from impedance data. In Table 3, such data are provided for the Ni/solution interface in the absence of adsorbates. However, the difference between C and $Y_{o,1}$ appears to be in fair analogy to the difference between unity and the corresponding values of CPE-1 exponent expressing the deviation of the Ni/solution interface from the ideally polarized condition.

Conclusions

Due to methanol self-dissociation, adsorbed NiOCH₃ is formed on the surface of anodically polarized polycrystalline Ni electrode in neutral anhydrous methanolic solutions, and it is reduced at negative potentials. The charging process of Ni electrode/methanolic solution interface is suggested to involve a double layer capacitive component and a non-capacitive

contribution due to the reduction of NiOCH_3 formed by irreversible adsorption of CH_3O^- species on the electrode surface.

Adsorbed tributylphosphine oxide, tri(*n*)octylphosphine oxide, and triphenylphosphine obey Langmuir isotherm, and the former two effectively inhibit $(\text{NiOCH}_3)_{\text{ads}}$ reduction within the potential range from 0.3 to -0.6 V vs. $\text{Ag}|\text{AgCl}$. Triphenylphosphine shows an apparent inhibitory effect on $(\text{NiOCH}_3)_{\text{ads}}$ reduction at low concentrations, but above 0.005 M, linear sweep voltammetry and electrochemical impedance analysis suggest for a faradaic process, identified with the one electron reduction of triphenylphosphine, which overlaps with $(\text{NiOCH}_3)_{\text{ads}}$ reduction.

Acknowledgments This work was financially supported by the Research Committee of Aristotle University of Thessaloniki, project number 89350.

References

- Horanyi E, Rizmayer EM (1984) *J Electroanal Chem* 180:97–108
- Zhou A, Xie N (1999) *J Colloid Interface Sci* 220:281–287
- Norton PR, Tapping RL (1976) *Chem Phys Lett* 38:207–212
- Cohen M, Merrill RP (1990) *Langmuir* 6:1282–1288
- Kwon H, Gewirth AA (2007) *J Electrochem Soc* 154:577–583
- Arvia AJ, Posadas D (1975) In: Bard AJ (ed) *Encyclopedia of electrochemistry of the elements*, vol. 3. Marcel Dekker, New York
- Inzelt G, Horanyi G (2006) In: Bard AJ, Stratmann M (eds) *Encyclopedia of electrochemistry*, vol. 7b. Inorganic chemistry. The Nickel Group, Wiley-VCH
- Bockris JO'M, Argade SD, Gileadi E (1969) *Electrochim Acta* 14: 1259–1283
- Devanathan MAV, Ramakrishnaiah K (1973) *Electrochim Acta* 18: 259–264
- Bockris JO'M, Potter EC (1952) *J Chem Phys* 20:614–628
- Anastopoulos AG, Moutzias I (1990) *J Electroanal Chem* 294: 143–150
- Nikitas P, Anastopoulos AG, Jannakoudakis D (1983) *J Electroanal Chem* 143:361–374
- Anastopoulos AG (1996) *Electrochim Acta* 41:2537–2544
- Anastopoulos AG, Paschalidou M, Papoutsis AD (2014) *J Electroanal Chem* 720–712:52–57
- Nikitas P, Anastopoulos AG, Jannakoudakis D (1983) *J Electroanal Chem* 145:407–421
- Anastopoulos AG, Christodoulou A, Jannakoudakis D (1983) *Z Phys Chem NF* 137:231–246
- Anastopoulos AG, Christodoulou A, Moutzias I (1988) *Can J Chem* 66:1053–1058
- Bozatzidis A, Anastopoulos AG, Laopoulos T (2007) *Electroanalysis* 19:1711–1718
- Trasatti S (1971) *J Electroanal Chem* 33:351–378
- Medway SL, Lucas CA, Kowal A, Nichols RJ, Johnson D (2006) *J Electroanal Chem* 587:172–181
- Miao Y, Ouyang L, Zhou S, Xu L, Yang Z, Xiao M, Ouyang R (2014) *Biosens Bioelectron* 53:428–439
- Banas J, Stypula B, Banas K, Swiatowska-Mrowiecka J, Starowicz M, Lelek-Borkowska U (2009) *J Solid State Electrochem* 13:1669–1679
- Shvarts E, Damaskin BB, Frumkin AN (1962) *Rus J Phys Chem* 36:1311–1315
- Frumkin AN (1967) *J Res Inst Catal Hokkaido Univ* 15:61–83
- Santhanam KSV, Bard AJ (1968) *J Am Chem Soc* 90:1118–1122
- Damaskin BB, Petrii O, Batrakov V (1971) *Adsorption of organic compounds on electrodes*. Plenum Press, New York
- Danilov F, Obratsov V, Kapitonov A (2003) *J Electroanal Chem* 552:69–76
- Lasia A (2014) *Electrochemical impedance spectroscopy and its applications*. Springer, New York
- Ragoisha GA (2015) *Electroanalysis* 27:855–863